

# An intercomparison of the deposition models used in the CASTNET and CAPMoN networks

Donna Schwede<sup>1</sup>

Atmospheric Modeling and Analysis Division, National Exposure Research Laboratory,  
U.S. Environmental Protection Agency  
Research Triangle Park, NC, USA 27711

Leiming Zhang

Air Quality Research Division, Science and Technology Branch,  
Environment Canada  
Toronto, Ontario, Canada M3H 5T4

Robert Vet

Air Quality Research Division, Science and Technology Branch,  
Environment Canada  
Toronto, Ontario, Canada M3H 5T4

Gary Lear

Clean Air Markets Division, Office of Air and Radiation,  
U.S. Environmental Protection Agency  
Washington, DC, USA 20005

March 9, 2011

---

<sup>1</sup> Corresponding author: Donna Schwede, USEPA, MD-E243-02, Research Triangle Park, NC, 27711,  
email: [Schwede.donna@epa.gov](mailto:Schwede.donna@epa.gov), phone: 919-541-3255, fax: 919-541-1379

## **Abstract**

To assess long-term trends in atmospheric deposition, the U.S. operates the Clean Air Status and Trends Network (CASTNET) and Canada operates the Canadian Air and Precipitation Monitoring Network (CAPMoN). Both networks use modeled dry deposition velocities and measured atmospheric concentrations to compute estimates of dry deposition. While concentration measurements from the two networks are comparable, flux estimates can be significantly different due to differences in the model-estimated dry deposition velocities. This study intercompares the dry deposition velocity models used by the networks to identify those model inputs and model algorithms that are responsible for the differences in the dry deposition velocity predictions of the gaseous trace species ozone ( $O_3$ ), sulfur dioxide ( $SO_2$ ), and nitric acid ( $HNO_3$ ). The Big-Leaf Model (BLM) used for CAPMoN was inserted into the CASTNET modeling framework so that the on-site meteorological data obtained at the CASTNET sites could be used as input to both models. The models were run for four CASTNET sites that spanned different land use types and climatologies. The models were incrementally modified to assess the impacts of algorithmic differences on the predicted deposition velocities. While differences in aerodynamic resistance between the models contributed strongly to differences in predicted dry deposition velocities for  $HNO_3$ , it is the non-stomatal (ground and cuticle) resistance parameterization that causes the largest differences for other chemical species. The study points to the need for further consideration of these resistances. Additionally, comparisons of both models against recent independent flux data are needed to assess the accuracy of the models.

Keywords: Atmospheric deposition, dry deposition, CASTNET, CAPMoN

## 1.0 Introduction

Atmospheric deposition is an important determinant of the pollutant budget in the atmosphere-biosphere system. Deposition of acidic species can result in the acidification of lakes and streams, adversely affecting sensitive ecosystems (Driscoll et al., 2001). In both the US and Canada, monitoring networks are in operation to study long-term trends in regional air quality and atmospheric deposition. The US EPA has operated the Clean Air Status and Trends Network (CASTNET) since 1991 (<http://java.epa.gov/castnet/>). The network consists of 87 sites located in rural areas which are located to minimize effects from local pollution sources. Continuous ozone ( $O_3$ ) measurements are reported as hourly concentrations and weekly concentration measurements using a filter pack are made of sulfur dioxide ( $SO_2$ ), nitric acid ( $HNO_3$ ), particulate sulfate ( $SO_4^{2-}$ ), nitrate ( $NO_3^-$ ), ammonium ( $NH_4^+$ ), and a suite of base cations. Additionally, continuous on-site meteorological measurements are taken at 10-m towers and ground-based sensors. Environment Canada operates the Canadian Air and Precipitation Monitoring Network (CAPMoN) which consists of 15 filter pack monitoring stations ([http://www.msc-smc.ec.gc.ca/capmon/Index\\_e.cfm](http://www.msc-smc.ec.gc.ca/capmon/Index_e.cfm)). A similar suite of atmospheric trace species is sampled at the CAPMoN sites with the addition of several nitrogen species at 3 sites.  $O_3$  is sampled continuously and reported hourly, while other pollutants are measured with 24-hour integrated filter samples. There is one co-located filter pack monitoring site between the CASTNET and CAPMoN networks which is located in Egbert, Ontario, Canada.

The approach taken to obtain estimates of dry deposition for network operations employs the inferential method (Hicks et al., 1985) where the measured concentration is paired with a modeled dry deposition velocity to compute the flux. For CASTNET, the dry deposition velocity for gases is calculated using the Multilayer Model (MLM) (Finkelstein et al., 2000; Meyers et al., 1998). When used operationally for CASTNET, the MLM uses the on-site meteorological data as input to its dry deposition velocity calculations. For CAPMoN, dry deposition velocities for gases are calculated using the Big Leaf Model (BLM) of Zhang et al. (2003b). The meteorological inputs used operationally for BLM are obtained from the Global Environmental Multiscale (GEM) meteorological model (Côté et al., 1998a; Côté et al., 1998b) since on-site meteorological data are not available at the CAPMoN sites.

To establish the comparability of the CASTNET and CAPMoN dry deposition estimates, their respective measured concentrations and modeled dry deposition velocities at the co-located Egbert site were compared for the period 2002-2007. The CAPMoN 24-hour-average measured concentrations and six-hour modeled dry deposition velocities of SO<sub>2</sub> and HNO<sub>3</sub> were converted to weekly-average concentrations and velocities corresponding to the CASTNET sampling weeks. The results, shown in Figures 1a and 1b, indicate that SO<sub>2</sub> and HNO<sub>3</sub> concentrations compare reasonably well, with a median % difference (i.e., Median of weekly values of  $[100 \times (\text{CASTNET} - \text{CAPMoN}) / (\text{CAPMoN})]$ ) between the two networks of -4.2% for SO<sub>2</sub> and -18.5% for HNO<sub>3</sub> (CAPMoN higher than CASTNET) and Pearson Correlation Coefficients of 0.98

and 0.90, respectively. In contrast, Figures 1c and 1d show that the estimated dry deposition fluxes of the two networks are substantially different, with the CAPMoN BLM-derived fluxes generally exceeding the CASTNET MLM fluxes (median % difference for SO<sub>2</sub> = -53.8% and for HNO<sub>3</sub> = -46.6%). Based on Figures 1e and 1f, these large differences between the estimated fluxes are predominantly due to differences in the BLM- and MLM-derived dry deposition velocities of SO<sub>2</sub> and HNO<sub>3</sub>, with median % differences of -49.3% and -34.7% for SO<sub>2</sub> and HNO<sub>3</sub>, respectively. While there is some degree of correlation between the HNO<sub>3</sub> deposition velocities, the SO<sub>2</sub> deposition velocities are essentially uncorrelated. Additionally, the range of weekly-average dry deposition velocities is quite different with CAPMoN SO<sub>2</sub> dry deposition velocities ranging from 0.15 to 0.88 cm s<sup>-1</sup> and CASTNET velocities ranging from 0.14 to 0.47 cm s<sup>-1</sup>. Similarly, the CAPMoN HNO<sub>3</sub> dry deposition velocities range from 0.49 to 3.17 cm s<sup>-1</sup> while the CASTNET velocities range from 0.50 to 1.87 cm s<sup>-1</sup>.

The dry deposition velocities from both models have been evaluated against field study data and have shown good agreement with the field study values, particularly for average diurnal cycles. For hourly values, the model performance is mixed. Meyers et al (1998) and Finkelstein et al (2000) compared the hourly deposition velocities from the MLM with measured data at five sites that included both crop covered and forested surfaces. For the crop surfaces, reported average mean biases in deposition velocity were 0.01 cm s<sup>-1</sup> for O<sub>3</sub>, -0.05 to 0.15 cm s<sup>-1</sup> for SO<sub>2</sub>, and 0.09 to 0.47 for HNO<sub>3</sub>. For tree surfaces, the average bias was -0.004 to 0.10 for O<sub>3</sub> and 0.21 to 0.25 for SO<sub>2</sub>. Evaluation of the BLM for O<sub>3</sub> and SO<sub>2</sub> is provided in Zhang et al (2002) and Zhang et al (2003a), respectively, for the same sites used in the MLM evaluations. Deposition velocities for

HNO<sub>3</sub> were not included in the BLM evaluation studies. The mean bias was not available from the BLM evaluations making it difficult to compare model performance with the MLM. However, correlation coefficients are provided for the BLM for O<sub>3</sub> and ranged from 0.43 to 0.75. Both models have been used to provide dry deposition estimates needed for follow-on studies such as ecological assessments (e.g. Lawrence et al., 2000; Mitchell et al., 2010). The choice of which modeled dry deposition velocity values to use could have large implications to pollutant budget calculations, leading to different conclusions from these ecological studies. It is important, therefore, to understand how differences in the model algorithms affect the calculated deposition velocities and the uncertainties associated with ecological assessments.

In this study we intercompare predicted hourly deposition velocities of O<sub>3</sub>, SO<sub>2</sub>, and HNO<sub>3</sub> from MLM and BLM to identify key differences in model inputs and algorithms that are responsible for the differences in predicted deposition velocities and ultimately estimates of flux. While both models also calculate deposition velocities of particulate matter using different algorithms, these differences are not addressed in this study. For this study, the BLM model was inserted into the framework used to run MLM to facilitate the use of consistent model inputs for both models. The models were analyzed to identify differences in model algorithms. Then, the models were incrementally modified to bring the model algorithms into agreement to allow quantification of the contribution of each model algorithm to the differences in calculated deposition velocities. In Section 2, an overview of the deposition models is provided. A description of the model

harmonization process is described in Section 3 and the results of the comparisons are presented in Section 4.

## 2.0 Overview of MLM and BLM Deposition Models

In this section, brief overviews of the MLM and BLM models are presented. More detailed information can be found in the cited references. Both models use the electrical resistance analogy to model the transfer of pollutants through the atmosphere to the surface where deposition velocity is calculated as the inverse of the sum of resistances that are combined in series or parallel.

### 2.1 Multilayer Model (MLM)

The Multilayer Model (MLM) includes the effects of aerodynamic resistance ( $R_a$ ), leaf boundary layer resistance ( $r_b$ ) and canopy resistance ( $r_c$ ). The leaf boundary resistance and the components of the canopy resistance are integrated from the surface to the mean height of the crown base to obtain the bulk canopy resistance. Deposition velocity ( $v_d$ ) is calculated from

$$v_d = \left( \frac{1}{\int_0^{h_c} r_c(z) dz + \frac{1}{r_{ac} + r_{soil}}} + R_a \right)^{-1} \quad (1)$$

and

$$r_c(z) = A(z) \left( \frac{1}{r_s(z) + r_b(z) + r_{mes}} + \frac{2}{r_b(z) + r_{cut}} \right) \quad (2)$$

where

$r_{ac}$	=	subcanopy aerodynamic resistance ( $\text{s m}^{-1}$ )
$r_{soil}$	=	soil resistance ( $\text{s m}^{-1}$ )
$A$	=	leaf area density ( $\text{m}^2 \text{m}^{-3}$ )
$r_s$	=	stomatal resistance ( $\text{s m}^{-1}$ )
$r_{mes}$	=	mesophyll resistance ( $\text{s m}^{-1}$ )
$r_{cut}$	=	cuticular resistance ( $\text{s m}^{-1}$ )
$h_c$	=	mean height of the crown base (m)

Aerodynamic resistance is parameterized as a function of the standard deviation of the wind direction ( $\sigma_\theta$ ) (Hicks et al., 1987), but modified to include an additional parameterization for nighttime low wind speed conditions. The friction velocity is then calculated using the approximation  $R_a \approx uu_*^{-2}$ . Leaf boundary layer resistance and canopy resistance are calculated at discrete levels within the canopy so that variations in wind speed and radiation within the canopy are considered. Stomatal resistance is calculated using the approach of Jarvis (1976) where  $r_s$  is determined from a plant species specific (rather than land use category specific) minimum stomatal resistance and factors that account for temperature, soil moisture, and vapor pressure deficit stresses. Soil moisture

stress is also used in the calculation of the soil resistance so that soluble species (e.g., SO<sub>2</sub>) are modeled as being more easily taken up by wet soils. Soil resistance also depends on the assumed pH of the soil surface with different values being used for forested and non-forested areas (Wesely, 1989). Cuticular resistance is a trace species specific value that varies with surface wetness.

## 2.2 Big-leaf Model (BLM)

The Big Leaf Model (BLM) considers the same resistances as MLM, but does not divide the canopy into layers. The canopy is, however, separated into shaded and sunlit portions (Zhang et al., 2003b) for the stomatal resistance calculation. Deposition velocity is calculated from

$$v_d = \frac{1}{R_a + R_b + R_c} \quad (3)$$

where  $R_b$  and  $R_c$  denote the bulk boundary layer and canopy resistances (s m<sup>-1</sup>). In addition to the resistances included in the canopy resistance in the MLM model (the notation is the same here except  $r$  has been replaced with  $R$  to indicate bulk properties for the canopy), BLM includes a stomatal blocking factor for wet conditions ( $W_{st}$ ):

$$\frac{1}{R_c} = \frac{1 - W_{st}}{R_s + R_m} + \frac{1}{R_{ac} + R_g} + \frac{1}{R_{cut}} \quad (4)$$

The aerodynamic resistance is calculated from similarity theory as in Padro et al. (1996) with the stability correction parameter derived from the bulk Richardson number.  $R_b$  is calculated as a function of friction velocity ( $u_*$ ). In contrast to the plant species specific approach of MLM, BLM recognizes 26 land use categories. Leaf Area Index (LAI), surface roughness, and stomatal resistance parameters are varied by land-use category in calculating the canopy resistance. Soil (ground) resistance is specified according to the trace species and land-use category and is modified for surface wetness. The cuticular resistance depends on the chemical, wetness of the surface, LAI, relative humidity and  $u_*$  (Zhang et al., 2003b).

### **3.0 Harmonization Methodology**

Differences in deposition velocity noted in Section 1 are due to a combination of differences in model input, including meteorology, site characteristics, plant parameters (e.g. leaf area index, canopy height, minimum stomatal resistance), and model algorithms. To the extent possible, the BLM and MLM deposition models were set up in this study to run with the same input parameters so that the focus of this analysis is on the differences in model algorithms. First, the models were configured to run from the same meteorological data to reduce differences associated with meteorological inputs. Next, differences in the parameterization of individual resistances were identified. Then, model resistance algorithms were incrementally modified to bring them into agreement with modifications being applied cumulatively. Changes in model-estimated deposition

velocities between runs reflect the sensitivity of the deposition algorithms to different formulations of a resistance. No preference was given to either model in the choice of resistance algorithms to be modified. The algorithm selected for use was based simply on convenience in code development. Tests on the ordering of modifications indicated little effect on the overall results and conclusions of the study. A summary description of the model runs is provided in Table 1.

Rather than focus only on the co-located site at Egbert, ON, several CASTNET sites were selected for use in this comparison. These sites spanned a range of climatologies and plant species. To simplify analyses, each site was modeled with only one plant species rather than the mix of species that actually exist at the site. Table 2 lists the locations of the sites and the plant species modeled at each site for this analysis.

Operationally, MLM is driven by meteorological parameters measured on-site at the CASTNET stations including hourly average wind speed and direction, standard deviation of the wind direction, air temperature at 2 and 9 m, solar radiation, relative humidity, precipitation, and surface wetness. Similar parameters, obtained from the GEM meteorological model, are used operationally as input to BLM for CAPMoN. For this analysis, BLM was inserted into the MLM framework so that both models could be run using the CASTNET meteorology. BLM requires both the ambient and surface temperatures to calculate the bulk Richardson number which is used to estimate  $R_a$  and  $u_*$ . So, the CASTNET framework and input meteorological data were modified slightly from the operational version to also include temperature at the 2 m level. There is no indication of seasonal snow cover in the CASTNET data, so deposition to snow was not considered by either model for this study while it is considered operationally for

CAPMoN. The models differ slightly in the way that leaf wetness is determined. CASTNET uses data from an on-site wetness sensor and contains an algorithm for estimating surface wetness (dew) if the data from the sensor are not available. BLM also contains a leaf wetness calculation, but the information from the on-site wetness sensor and MLM method for filling missing wetness data were used for both models to provide consistency. For most hours (80%), both the sensor and the BLM calculation gave similar indications of the presence of dew.

#### 4.0 Results

The modeling framework was run for a multiyear time period for each site to allow spin-up of the soil moisture budget for MLM. One year of each run was selected for each site, based on data completeness, for further analysis. The model intercomparison results are discussed in detail below with each section focusing on a particular set of model parameterizations. Modeled hourly deposition velocities were paired and the mean difference ( $MD$ ), mean absolute difference ( $MAD$ ), and Pearson correlation coefficient ( $R$ ) were calculated for the one year period as follows:

$$MD = \frac{\sum_1^N (BLM - MLM)}{N} \quad (5)$$

$$MAD = \frac{\sum_1^N (|BLM - MLM|)}{N} \quad (6)$$

$$R = \frac{N \sum_1^N (MLM * BLM) - \left( \sum_1^N MLM \right) \left( \sum_1^N BLM \right)}{\left( N \sum_1^N MLM^2 - \left( \sum_1^N MLM \right)^2 \right)^{0.5} * \left( N \sum_1^N BLM^2 - \left( \sum_1^N BLM \right)^2 \right)^{0.5}} \quad (7)$$

Table 3 presents a summary of these values for each trace species for each model configuration. Comparisons of the general distribution of the hourly model predictions are also of interest. These results are presented as box plots (Figures 2-4) while numerical values are included in the supplementary data. In these figures, the box provides the interquartile range, a horizontal line indicates the median, the mean is indicated by an X, the whiskers show the 5-95 percentile range and circles show outliers of the distribution of the hourly deposition velocity values. The key to the abbreviations for the model runs can be found in Table 1.

#### 4.1 Base case

An initial run of the modeling system was done with both models using their native algorithms for all resistances. The first goal of this run (Base) was to see if the hourly results of runs across all sites used in this study were consistent with the differences noted in Section 1 for the weekly values based on operational data for the Egbert site, once consistent meteorology was used to drive the models. Scatter plots of hourly deposition velocities calculated for the base case runs for EGB181 (not shown) are similar to the weekly values shown in Figure 1 for SO<sub>2</sub> with the mean hourly  $v_d$  calculated by BLM (0.48) being higher than that calculated using MLM (0.18). Figure

4b shows that for HNO<sub>3</sub>, the  $v_d$ 's from BLM are higher than those from MLM, but the hourly data range and average values for the models are more similar in the base case in comparison to the weekly results shown in Figure 1. This is likely due to the change in input meteorology, particularly wind speed which affects the aerodynamic resistance and is the primary driver for the HNO<sub>3</sub>  $v_d$ . The wind speed used operationally for CAPMoN is from the GEM model lowest level which is typically at 40-50 m whereas in this study the wind speed measured at 10 m was used as input to both models. The second goal for the base case was to establish the benchmark for the start of the incremental modifications described in subsequent sections. For BVL130 and SUM156, the mean O<sub>3</sub>, and SO<sub>2</sub>, deposition velocities are a factor of 1.5 to 3 higher for BLM in comparison to the MLM values for the base case (Figures 2-3). At these same sites, the HNO<sub>3</sub> deposition velocities for BLM are also higher than for MLM for the base case; however, at the SND152, the MLM mean  $v_d$ 's for each trace species are generally higher than the corresponding BLM values (Figures 2-4).

#### 4.2 Leaf Area Index and plant parameters

Leaf Area Index (LAI) is an important input to deposition models as it has a strong influence on the canopy resistance (Cooter and Schwede, 2000). For MLM usage in CASTNET, LAI is determined from site-specific leaf-out schedules for each plant which are specified based on measurements taken during 1991 and 1992 (Clarke et al., 1997). The same leaf-out schedules is used for each year, regardless of meteorological conditions. For BLM usage in CAPMoN, LAI is determined from a land use category

specific leaf-out schedule. The same leaf-out schedule is used at all sites and is not affected by interannual variations in meteorology or by site location. Plots of the annual time series of LAI values are provided in the supplementary data. LAI values for the BVL130 and EGB181 sites calculated by the operational approaches for the two networks were quite similar in maximum LAI and timing of peak LAI. The two model approaches produce LAI values for the SND152 site, and particularly the SUM156 site that are quite different from one another. To test the effect of estimated LAI value differences on the predicted deposition velocities between the two models, we modified the code to use the LAI from BLM for both models (run LAI). This change resulted in lower *MAD*'s (Table 3), particularly for O<sub>3</sub>, and most notably at the EGB181, SND152, and SUM156 sites where the differences in the base values of the LAI between the models were greatest. Correlation coefficients were relatively unaffected (< 5% change) by the change in LAI. The effects of the change in LAI on the distributions of the deposition velocity estimates are most evident for O<sub>3</sub> for SND152 and SUM156. At SND152, the mean MLM deposition velocity decreased from 0.31 to 0.25 cm s<sup>-1</sup> and the 75<sup>th</sup> percentile value decreased from 0.53 to 0.37 cm s<sup>-1</sup> due to the decrease in LAI when the BLM value of LAI was substituted for the MLM one. For the SUM156 site, the mean MLM  $v_d$  increased from 0.18 to 0.23 cm s<sup>-1</sup> because the LAI increased by a factor of 1.6 to 2.0 when the BLM LAI was used in place of the MLM value.

A second aspect of the plant-specific model inputs are the plant parameters that are input to the stomatal flux formulations. These parameters include the minimum stomatal resistance for water vapor ( $r_{smin}$ ), the light response parameter, and minimum, maximum, and optimal temperatures for stomatal opening. For this test, the code was

modified so that the plant parameter values from the MLM model were used to drive both models (run PP). This change had no effect at the BVL130 site as the parameters for corn were not changed. For other sites and trace species, the greatest changes were made in the minimum stomatal resistance and resulted in lower values of  $r_{min}$  being used for BLM compared to the base case (not shown). This increased the deposition velocities predicted by BLM. Mean differences increased with the greatest change occurring for O<sub>3</sub> for the SND152 site where the  $MD$  increased from .002 to 0.06 cm s<sup>-1</sup>, but correlation coefficients also increased by about 5%. Using SND152 as an example, we can use the distribution information in Figures 2-4 to see that differences in the high end of the distribution are likely affecting the mean difference statistic, but the bulk of the distribution show little change. After these harmonization steps, there are still clear differences in the estimated deposition velocities suggesting that these parameters may not be the key sensitivities driving these differences.

#### 4.3 Aerodynamic resistance and friction velocity

MLM and BLM use different formulations for the aerodynamic resistance due to the meteorological inputs available from the different network operations. First, the differences in the  $R_a$ 's predicted by the two models were examined (see supplementary data). Generally, the aerodynamic resistance calculated by the MLM model was greater than that calculated by the BLM model for the same hour. Some values of  $R_a$  calculated by MLM exceeded 100000 s m<sup>-1</sup> with a corresponding value of  $u_*$  of 0.0002 while BLM limits  $R_a$  to 1000 s m<sup>-1</sup> and corresponding values for  $u_*$  are on the order of 0.02. The

highest values for  $R_a$  calculated by the MLM model are associated with nighttime low wind speed conditions. Previous comparisons of  $R_a$  parameterizations (Liu et al., 2007; Padro et al., 1994) have shown a wide range of values of  $R_a$  predicted by various models, so differences between the values predicted by MLM and BLM are not unexpected.

For this analysis, a limit of  $1000 \text{ s m}^{-1}$  was implemented in the MLM code to prevent exceptionally high values of  $R_a$  and corresponding extremely low values of  $u^*$  from dominating the results as other resistances rely on  $u^*$ , particularly in BLM. The BLM code was then modified to use this revised  $R_a$  calculated by MLM (run Ra). As expected, the change in  $R_a$  and  $u^*$  had the greatest effect on the  $\text{HNO}_3$   $v_d$ 's because  $\text{HNO}_3$  deposits readily to surfaces (surface resistance is low). In Figure 4, the results of capping the value for  $R_a$  can be seen by closely comparing the outliers in the lower tail of the distribution of the deposition velocities from MLM for runs PP and Ra. An appreciable shift in the distributions of the BLM  $\text{HNO}_3$  deposition velocities can be seen as a result of the change in  $R_a$  and  $u^*$  from the native BLM values to the MLM values can also be seen in Figure 4. For the BVL130, EGB181, and SUM156 sites, the mean  $v_d$  decreased markedly. In comparison to the other sites, SND152 has a higher number of hours for which the  $R_a$  from the BLM parameterization is higher than the  $R_a$  from the MLM parameterization, so changing to the MLM parameterization increases the mean  $v_d$  for this site. For all sites, the *MAD* is notably lower and the correlation coefficient is substantially higher for the paired  $\text{HNO}_3$   $v_d$ 's in comparison to the LAI run indicating better overall agreement between the paired deposition velocities when the same value of  $R_a$  is used in both models. Clearly the differences in the  $R_a$  parameterization contribute strongly to the overall differences in the  $v_d$ , particularly for  $\text{HNO}_3$ .

#### 4.4 Stomatal resistance factors

Both MLM and BLM calculate the stomatal resistance using the Jarvis approach (Jarvis, 1976) where a specified minimum stomatal resistance is modified due to environmental stress factors including temperature, solar radiation, vapor pressure deficit, and soil moisture. The temperature factor is the same in both models. MLM and BLM use the same basis for calculating the radiation factor, but MLM applies the radiation model at each level in the canopy and BLM applies it to the bulk canopy. The vapor deficit factor ( $f_v$ ) is calculated in both models from  $f_v = 1 - b_{vpd}(e_l - e_{sfc})$ , where  $e_l$  is the vapor pressure inside the stomata and  $e_{sfc}$  is the vapor pressure at the leaf surface and  $b_{vpd}$  is a constant. The models differ in the value of  $b_{vpd}$  as MLM uses a constant value of 0.02 and BLM uses a land-use category specific value (e.g. 0.0 for crops and grass, 0.036 for deciduous forest) and in that MLM calculates  $f_v$  at each level in the canopy. To test the effect of differences in the value of  $b_{vpd}$ , BLM was modified to use the constant value of 0.02 (run Fv). The change in  $b_{vpd}$  had little effect on the overall distribution of BLM  $v_d$ 's (Figures 2-4) and produced only subtle changes in the statistical measures shown in Table 3. The soil moisture stress factor,  $f_w$ , is also different between the models. MLM uses a simple evapotranspiration model to track the soil moisture budget to determine the stress factor while the stress factor for BLM is a function of solar radiation. Although there are clear differences between the soil moisture stress factors calculated by the two models, harmonizing these algorithms (run Fs) resulted in little impact on the calculated deposition velocities at most sites as evidenced by the comparing the results of the Fv and

Rs runs presented in Figures 2-4. There is more of an effect at the Egbert site, where the *MAD* for O<sub>3</sub> decreased from 0.09 to 0.06, because the MLM evapotranspiration approach indicates that 1999 was a relatively dry year while the BLM parameterization does not indicate any moisture stress. The O<sub>3</sub> deposition velocities were more impacted by this change than the SO<sub>2</sub> and HNO<sub>3</sub> deposition velocities (Table 3), as expected given the strong dependence of O<sub>3</sub> deposition on stomatal resistance.

#### 4.5 In-canopy aerodynamic resistance and ground (soil) resistance

The deposition pathway to the soil is modeled in both MLM and BLM as two resistances, the in-canopy aerodynamic resistance and the ground (soil) resistance, acting in series; however, the parameterization of these resistances differs between the models. The in-canopy aerodynamic resistance in BLM varies with land use category and is a function of LAI and  $u^*$ . In MLM, this resistance is a function of the wind speed and the canopy height and roughness length for the plant species. Generally, the in-canopy aerodynamic resistance calculated by BLM was much higher than that calculated by MLM for a given hour and hours with low values of  $u^*$  resulted in values for the in-canopy aerodynamic resistance for BLM of over  $10^6$ . For this test, the MLM code was modified to use the BLM value of the resistance (run Rac). Overall, the change in the in-canopy resistance resulted in lower mean absolute differences. This change made a particularly notable difference in the magnitude and sign of the mean difference for SO<sub>2</sub>  $v_d$  for the BVL130 (-0.11 vs. 0.03) and the SND152 (-0.17 vs. 0.43 cm s<sup>-1</sup>) sites compared to the results from run Rs (Table 3). Since the resistance was increased in MLM

compared to the Rs run, the MLM deposition velocities decreased as indicated in the distributions in Figures 2-4 with the greatest change occurring for the SO<sub>2</sub> and HNO<sub>3</sub>  $v_d$ 's. For the EGB181 and SUM156 sites, the impact on the distributions was minimal (Figures 2-4).

In MLM, the ground or soil resistance is a constant value for O<sub>3</sub> and HNO<sub>3</sub>. For SO<sub>2</sub>, an initial value is modified by the soil moisture to account for differences in uptake by wet and dry soils. The BLM model follows a similar approach, but varies the values by land-use category as well. An important distinction between the models is that soil wetness is determined from the soil moisture budget in MLM while in BLM soil wetness is determined by the presence of dew and rain (> 2.5 mm/h) since a soil moisture budget is not available. In this test (run Rg), MLM was modified to use the ground resistance calculated by BLM. This change made a notable difference in the degree of agreement between the models for most sites for O<sub>3</sub> and SO<sub>2</sub> as indicated by the decreases in *MAD* and increase in *R* in Table 3 relative to the Rac run. For example, the *R* for O<sub>3</sub> at the BVL130 site increased from 0.64 to 0.98 with a corresponding decrease in the *MAD* from 0.09 to 0.01. The operational values of the soil resistance for O<sub>3</sub> for MLM are a factor of 2-3 higher than those for BLM. Using the BLM value for the soil resistance resulted in an increase in the MLM predicted deposition velocities which brought the distributions of hourly  $v_d$ 's into better agreement (Figures 2-4). For SO<sub>2</sub>, no consistent bias is evident in the operational soil resistance values, so changing from the MLM approach to the BLM approach yielded mixed results. The degree of impact of changing approaches will differ with the precipitation and soil moisture budget. For example, a site with near-drought conditions would have a high soil resistance under the MLM approach and a dew

occurrence would not influence the value. However, the dew occurrence would result in a low soil resistance for SO<sub>2</sub> under the BLM approach.

#### 4.6 Cuticle resistance

Similar to the soil resistance, the cuticular resistance also depends on surface wetness and separate values are given for dry, rain-wetted and dew-wetted surfaces in both models. The distinction between rain and dew wetted surfaces accounts for differences in the pH of rainwater and dew. In MLM, there are three possible values for the cuticular resistance, depending on the wetness and origin of the wetness. In BLM, an initial value of the cuticular resistance is selected for a given land use and is modified based on the LAI,  $u^*$ , and relative humidity with different formulas used for the various depositing trace species and wetness origins. A comparison of the cuticular resistances from the models showed no correlation between the values (see supplementary data). For this test, the MLM code was modified to use the BLM value for the cuticular resistance (run Rcut). Figures 2-4 show the dramatic effect that changing the cuticular resistance had on the distribution of the hourly deposition velocities. Changes in the distributions were driven by a large number of hours where the cuticular resistance for MLM was substantially reduced (e.g. from 10000 to 24 s m<sup>-1</sup>) which resulted in much higher values of  $v_d$ . The bottom half of the distribution showed little change since those hours are dominated by higher cuticular resistances which effectively shut down that pathway of deposition. Clearly further study of these two very different cuticular resistance approaches is warranted.

## 5.0 Summary

Atmospheric deposition contributes about 30% to the overall nitrogen budget (Boyer et al., 2002) and as much as 80% to the sulfur budget (Likens et al., 2002; Mitchell et al., 1986; Shanley et al., 2005) in watersheds. Measurements of dry deposition are technically challenging and expensive, so modeled deposition velocities are paired with measured concentrations to determine fluxes for long term monitoring networks such as CASTNET and CAPMoN. Since many approaches are available to obtain the deposition velocity and, therefore, the flux, characterizing the uncertainty associated with atmospheric deposition estimates becomes important to pollutant budget studies. For example, Mitchell et al (2010) found that uncertainties in atmospheric deposition could affect conclusions regarding whether a watershed was retaining or releasing sulfur, which affects management strategies. Results of the current study also provide relevant input to the characterization of uncertainty for exposure assessments. For example, given consistent meteorological inputs and site characterization (e.g. vegetation type, LAI, canopy height, surface roughness), the median hourly  $v_d$  and, therefore, the flux can be a factor of 2-3 different depending on the choice of deposition velocity model. Using these different flux values in exposure assessments would lead to different conclusions regarding the likelihood of damage to plants from exposure to high levels of O<sub>3</sub>.

The current study has illustrated some of the key differences between model inputs and parameterizations used to estimate dry deposition velocities for the CASTNET and CAPMoN networks. While concentration measurements from these networks are in

good agreement, the deposition velocities are quite different and indicate areas for model improvement. This study concludes that differences in meteorological inputs and the formulation of the aerodynamic resistance have a strong influence on the calculated deposition velocity of HNO<sub>3</sub>. For O<sub>3</sub> and SO<sub>2</sub>, the differences in deposition velocity estimates are dominated by differences in ground (soil) and cuticular resistances. These resistances are not well measured or understood and this study points to the need for further consideration of these resistances. While it is important to understand the dominance of these factors on the MLM and BLM deposition velocity differences, it still remains unclear how accurate the two models are. Follow-on work will focus on comparisons of the models against multi-year flux data.

## **6.0 Acknowledgements**

The authors gratefully acknowledge the contributions of the CASTNET and CAPMoN networks, the assistance of Mike Shaw of Environment Canada for calculating the CAPMoN estimates and providing diagrams and the helpful insights from Tilden Meyers on the details of the MLM model. Review comments provided by Joseph Sickles and John Walker led to improvements in the paper. The United States Environmental Protection Agency through its Office of Research and Development collaborated in the research described here. It has been subjected to Agency review and approved for publication.

## **7.0 References**

- Boyer, E.W., Goodale, C.L., Jaworski, N.A. and Howarth, R.W., 2002. Anthropogenic nitrogen sources and relationships to riverine nitrogen export in the northeastern U.S.A. *Biogeochemistry*, 57-58(1): 137-169.
- Clarke, J.F., Edgerton, E.S. and Martin, B.E., 1997. Dry deposition calculations for the Clean Air Status and Trends Network. *Atmospheric Environment*, 31(21): 3667-3678.
- Cooter, E.J. and Schwede, D.B., 2000. Sensitivity of the National Oceanic and Atmospheric Administration multilayer model to instrument error and parameterization uncertainty. *Journal of Geophysical Research-Atmospheres*, 105(D5): 6695-6707.
- Côté, J. et al., 1998a. The Operational CMC-MRB Global Environmental Multiscale (GEM) Model. Part II: Results. *Monthly Weather Review*, 126(6): 1397-1418.
- Côté, J. et al., 1998b. The Operational CMC-MRB Global Environmental Multiscale (GEM) Model. Part I: Design Considerations and Formulation. *Monthly Weather Review*, 126(6): 1373-1395.
- Driscoll, C.T. et al., 2001. Acidic deposition in the northeastern United States: Sources and inputs, ecosystem effects, and management strategies. *Bioscience*, 51(3): 180-198.
- Finkelstein, P.L. et al., 2000. Ozone and sulfur dioxide dry deposition to forests: Observations and model evaluation. *Journal of Geophysical Research*, Washington, DC. Vol. 105(D12): 15365-15377.
- Hicks, B.B. et al., 1985. On the use of monitored air concentrations to infer dry deposition. NOAA Tech. Memo, pp. 65.
- Hicks, B.B., Baldocchi, D.D., Meyers, T.P., Hosker, R.P. and Matt, D.R., 1987. A preliminary multiple resistance routine for deriving dry deposition velocities from measured quantities. *Water, Air, & Soil Pollution*, V36(3): 311-330.
- Jarvis, P.G., 1976. The Interpretation of the Variations in Leaf Water Potential and Stomatal Conductance Found in Canopies in the Field. *Philosophical Transactions of the Royal Society of London. Series B, Biological Sciences*, 273(927): 593-610.
- Lawrence, G.B., Lovett, G.M. and Baevsky, Y.H., 2000. Atmospheric deposition and watershed nitrogen export along an elevational gradient in the Catskill Mountains, New York. *Biogeochemistry*, 50(1): 21-43.
- Likens, G.E. et al., 2002. The biogeochemistry of sulfur at Hubbard Brook. *Biogeochemistry*, 60(3): 235-316.
- Liu, S., Lu, L., Mao, D. and Jia, L., 2007. Evaluating parameterizations of aerodynamic resistance to heat transfer using field measurements. *Hydrol. Earth Syst. Sci.*, 11(2): 769-783.
- Meyers, T.P., Finkelstein, P., Clarke, J., Ellestad, T.G. and Sims, P.F., 1998. A multilayer model for inferring dry deposition using standard meteorological measurements. *Journal of Geophysical Research*, 103(D17): 22645-22661.
- Mitchell, M. et al., 2010. Comparisons of watershed sulfur budgets in Southeast Canada and northeast US: new approaches and implications. Accepted for Publication in *Biogeochemistry*.

- Mitchell, M.J., David, M.B., Maynard, D.G. and Telang, S.A., 1986. Sulfur constituents in soils and streams of a watershed in the Rocky Mountains of Alberta. *Canadian Journal of Forest Research*, 16: 315-320.
- Padro, J., 1996. Summary of ozone dry deposition velocity measurements and model estimates over vineyard, cotton, grass and deciduous forest in summer. *Atmospheric Environment*, 30(13): 2363-2369.
- Padro, J., Massman, W.J., Shaw, R.H., Delany, A. and Oncley, S.P., 1994. A comparison of some aerodynamic resistance methods using measurements over cotton and grass from the 1991 California ozone deposition experiment. *Boundary-Layer Meteorology*, 71(4): 327-339.
- Shanley, J.B. et al., 2005. Tracing sources of streamwater sulfate during snowmelt using S and O isotope ratios of sulfate and S-35 activity. *Biogeochemistry*, 76(1): 161-185.
- Wesely, M.L., 1989. Parameterization of surface resistances to gaseous dry deposition in regional-scale numerical models. *Atmospheric Environment* (1967), 23(6): 1293-1304.
- Zhang, L., Brook, J.R. and Vet, R., 2002. On ozone dry deposition--with emphasis on non-stomatal uptake and wet canopies. *Atmospheric Environment*, 36(30): 4787-4799.
- Zhang, L., Brook, J.R. and Vet, R., 2003a. Evaluation of a non-stomatal resistance parameterization for SO<sub>2</sub> dry deposition. *Atmospheric Environment*, 37(21): 2941-2947.
- Zhang, L., Brook, J.R. and Vet, R., 2003b. A revised parameterization for gaseous dry deposition in air-quality models. *Atmospheric Chemistry and Physics*, 3(6): 2067-2082.

## List of Tables

Table 1. Description of the model configurations used in the study.

Table 2. Site locations and modeled vegetation types.

Table 3. Mean difference ( $\text{cm s}^{-1}$ ), mean absolute difference ( $\text{cm s}^{-1}$ ), and Pearson correlation coefficients for paired model-estimated hourly deposition velocities for each model configuration.

## List of Figures

Figure 1. Comparison of operational values from the CASTNET and CAPMoN networks for weekly values of (a) measured SO<sub>2</sub> concentration ( $\mu\text{g m}^{-3}$ ), (b) measured HNO<sub>3</sub> concentration ( $\mu\text{g m}^{-3}$ ), (c) estimated SO<sub>2</sub> flux ( $\text{kg ha}^{-1}$ ), (b) estimated HNO<sub>3</sub> flux ( $\text{kg ha}^{-1}$ ), (e) modeled SO<sub>2</sub> deposition velocity ( $\text{cm s}^{-1}$ ), and (f) modeled HNO<sub>3</sub> deposition velocity ( $\text{cm s}^{-1}$ ).

Figure 2. Ozone deposition velocity distributions for (a) BVL130, (b) EGB181, (c) SND152, and (d) SUM156 for different model configurations. White bars indicate values from MLM and grey bars indicate values from BLM. The abbreviations for the model configurations (x-axis) are provided in Table 1.

Figure 3. Sulfur dioxide deposition velocity distributions for (a) BVL130, (b) EGB181, (c) SND152, and (d) SUM156 for different model configurations. White bars indicate values from MLM and grey bars indicate values from BLM. The abbreviations for the model configurations (x-axis) are provided in Table 1.

Figure 4. Nitric acid deposition velocity distributions for (a) BVL130, (b) EGB181, (c) SND152, and (d) SUM156 for different model configurations. White bars indicate values from MLM and grey bars indicate values from BLM. The abbreviations for the model configurations (x-axis) are provided in Table 1.

Table 1. Description of the model configurations used in the study.

Run Name	Description
Base	Both MLM and BLM run in their native configuration using on-site meteorology from CASTNET
LAI	As with the Base run except MLM was modified to use the LAI from BLM
PP	As with the LAI run except BLM was modified to use the MLM plant parameters
Ra	As with the PP run except BLM was modified to use the MLM aerodynamic resistance
Fv	As with the Ra run except BLM was modified to use the MLM vapor pressure deficit function in the stomatal resistance calculation
Rs	As with the Fv run except BLM was modified to use the MLM water stress function in the stomatal resistance calculation
Rac	As with the Rs run except MLM was modified to use the BLM in-canopy aerodynamic resistance
Rg	As with the Rac run except MLM was modified to use the BLM ground (soil) resistance
Rcut	As with the Rg run except MLM was modified to use the BLM cuticular resistance

Table 2. Site locations and modeled vegetation types.

Site ID	Year for analysis	Location	Latitude	Longitude	Vegetation type
BVL130	1998	Bondville, IL	40.0519	-88.3724	Maize
EGB181	1999	Egbert, ON	44.232	-79.7812	Sugar Maple
SND152	1994	Sand Mt, AL	34.2888	-85.9698	Grass
SUM156	1997	Sumatra, FL	30.1103	-84.9903	Loblolly Pine

Table 3. Mean difference ( $\text{cm s}^{-1}$ ), mean absolute difference ( $\text{cm s}^{-1}$ ), and Pearson correlation coefficients for paired model-estimated hourly deposition velocities for each model configuration.

Site	Run Name	$\text{O}_3$			$\text{SO}_2$			$\text{HNO}_3$		
		Mean Diff.	Mean Abs. Diff.	Correl. Coeff.	Mean Diff.	Mean Abs. Diff.	Correl. Coeff.	Mean Diff.	Mean Abs. Diff.	Correl. Coeff.
BVL130	Base	0.201	0.204	0.335	0.079	0.187	0.323	0.426	0.827	0.084
BVL130	LAI	0.188	0.194	0.381	0.084	0.187	0.322	0.405	0.840	0.085
BVL130	PP	0.188	0.194	0.381	0.084	0.187	0.323	0.405	0.841	0.085
BVL130	Ra	0.069	0.091	0.636	-0.097	0.120	0.771	-0.286	0.289	0.913
BVL130	Fv	0.062	0.085	0.582	-0.102	0.123	0.760	-0.288	0.291	0.909
BVL130	Rs	0.056	0.084	0.533	-0.107	0.126	0.769	-0.289	0.292	0.907
BVL130	Rac	0.075	0.085	0.641	0.028	0.046	0.835	-0.140	0.183	0.880
BVL130	Rg	-0.006	0.013	0.982	0.030	0.032	0.923	-0.166	0.178	0.917
BVL130	Rcut	-0.061	0.061	0.826	-0.094	0.099	0.844	-0.084	0.129	0.944
EGB181	Base	0.120	0.136	0.746	0.255	0.266	0.483	0.624	0.892	0.500
EGB181	LAI	0.104	0.124	0.786	0.242	0.255	0.501	0.470	0.870	0.484
EGB181	PP	0.129	0.145	0.834	0.263	0.274	0.568	0.479	0.870	0.492
EGB181	Ra	0.008	0.074	0.873	0.051	0.106	0.723	-0.535	0.541	0.832
EGB181	Fv	0.028	0.087	0.895	0.068	0.118	0.774	-0.526	0.533	0.850
EGB181	Rs	-0.024	0.063	0.863	0.024	0.085	0.675	-0.544	0.551	0.819
EGB181	Rac	0.016	0.050	0.891	0.087	0.095	0.708	-0.360	0.467	0.776
EGB181	Rg	-0.008	0.030	0.959	0.067	0.075	0.794	-0.362	0.466	0.779
EGB181	Rcut	-0.116	0.123	0.853	-0.191	0.210	0.878	-0.133	0.339	0.814
SND152	Base	-0.057	0.133	0.788	-0.306	0.320	0.776	-0.767	0.846	0.685
SND152	LAI	0.002	0.087	0.854	-0.277	0.291	0.798	-0.696	0.776	0.714
SND152	PP	0.059	0.089	0.902	-0.229	0.253	0.808	-0.682	0.764	0.730
SND152	Ra	0.122	0.150	0.918	-0.151	0.179	0.912	-0.431	0.432	0.965
SND152	Fv	0.101	0.130	0.909	-0.169	0.189	0.912	-0.438	0.438	0.962
SND152	Rs	0.094	0.123	0.912	-0.174	0.187	0.931	-0.439	0.439	0.961
SND152	Rac	0.114	0.121	0.929	0.043	0.077	0.943	-0.160	0.185	0.964
SND152	Rg	0.019	0.029	0.994	0.080	0.083	0.979	-0.198	0.202	0.973
SND152	Rcut	-0.040	0.042	0.981	-0.084	0.085	0.972	-0.061	0.102	0.982
SUM156	Base	0.087	0.127	0.671	0.178	0.217	0.433	0.193	0.894	0.584
SUM156	LAI	0.042	0.120	0.703	0.145	0.209	0.446	0.036	0.982	0.574
SUM156	PP	0.054	0.110	0.778	0.156	0.205	0.501	0.040	0.979	0.579
SUM156	Ra	-0.058	0.079	0.921	-0.026	0.092	0.826	-0.669	0.669	0.916
SUM156	Fv	-0.041	0.072	0.932	-0.011	0.088	0.854	-0.663	0.663	0.923
SUM156	Rs	-0.058	0.068	0.962	-0.026	0.080	0.868	-0.668	0.668	0.919
SUM156	Rac	-0.033	0.049	0.966	0.026	0.067	0.865	-0.640	0.640	0.920
SUM156	Rg	-0.044	0.052	0.975	0.020	0.064	0.873	-0.640	0.640	0.919
SUM156	Rcut	-0.327	0.327	0.949	-0.433	0.433	0.974	-0.506	0.506	0.953

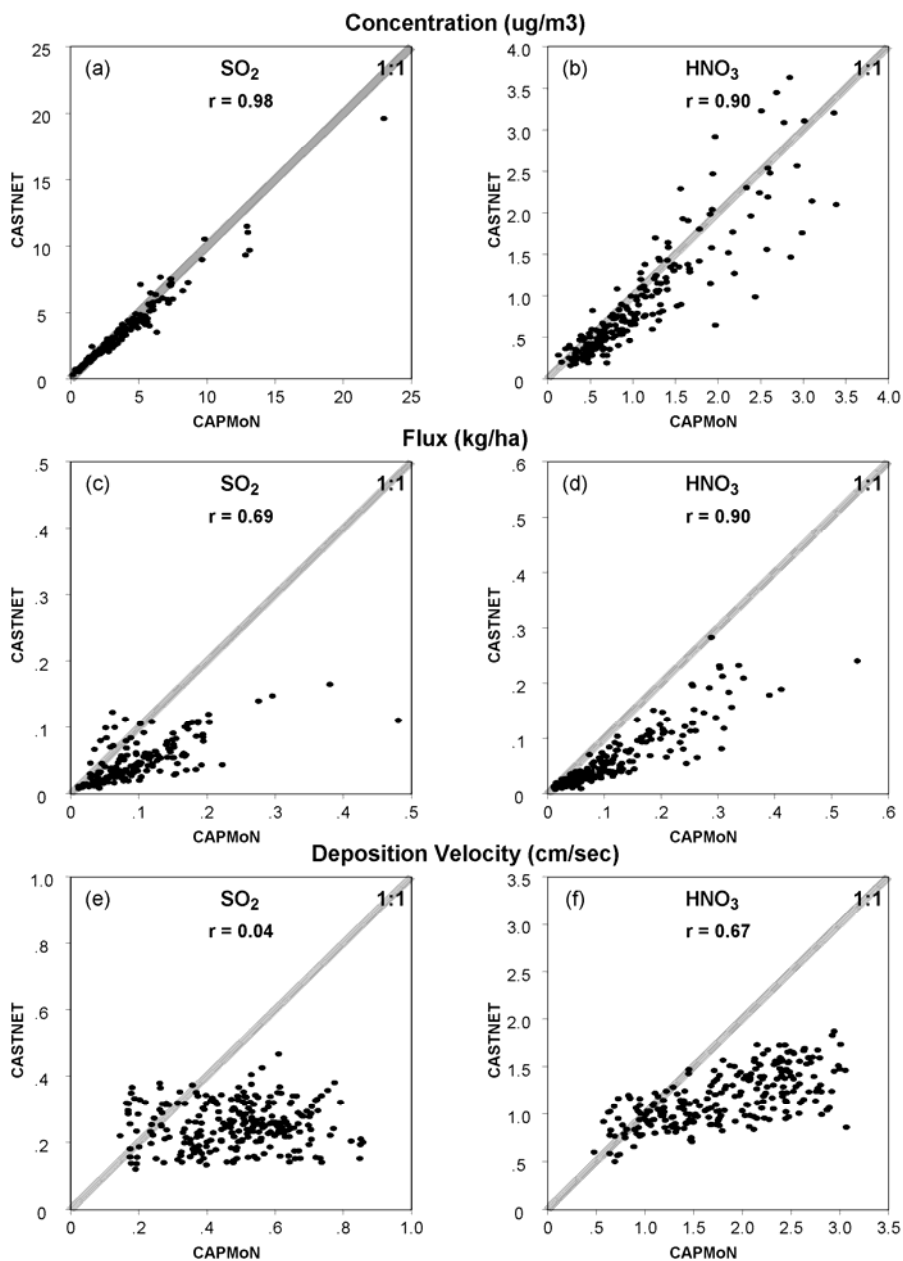


Figure 1. Comparison of operational values from the CASTNET and CAPMoN networks for weekly values of (a) measured SO<sub>2</sub> concentration ( $\mu\text{g m}^{-3}$ ), (b) measured HNO<sub>3</sub> concentration ( $\mu\text{g m}^{-3}$ ), (c) estimated SO<sub>2</sub> flux ( $\text{kg ha}^{-1}$ ), (d) estimated HNO<sub>3</sub> flux ( $\text{kg ha}^{-1}$ ), (e) modeled SO<sub>2</sub> deposition velocity ( $\text{cm s}^{-1}$ ), and (f) modeled HNO<sub>3</sub> deposition velocity ( $\text{cm s}^{-1}$ )

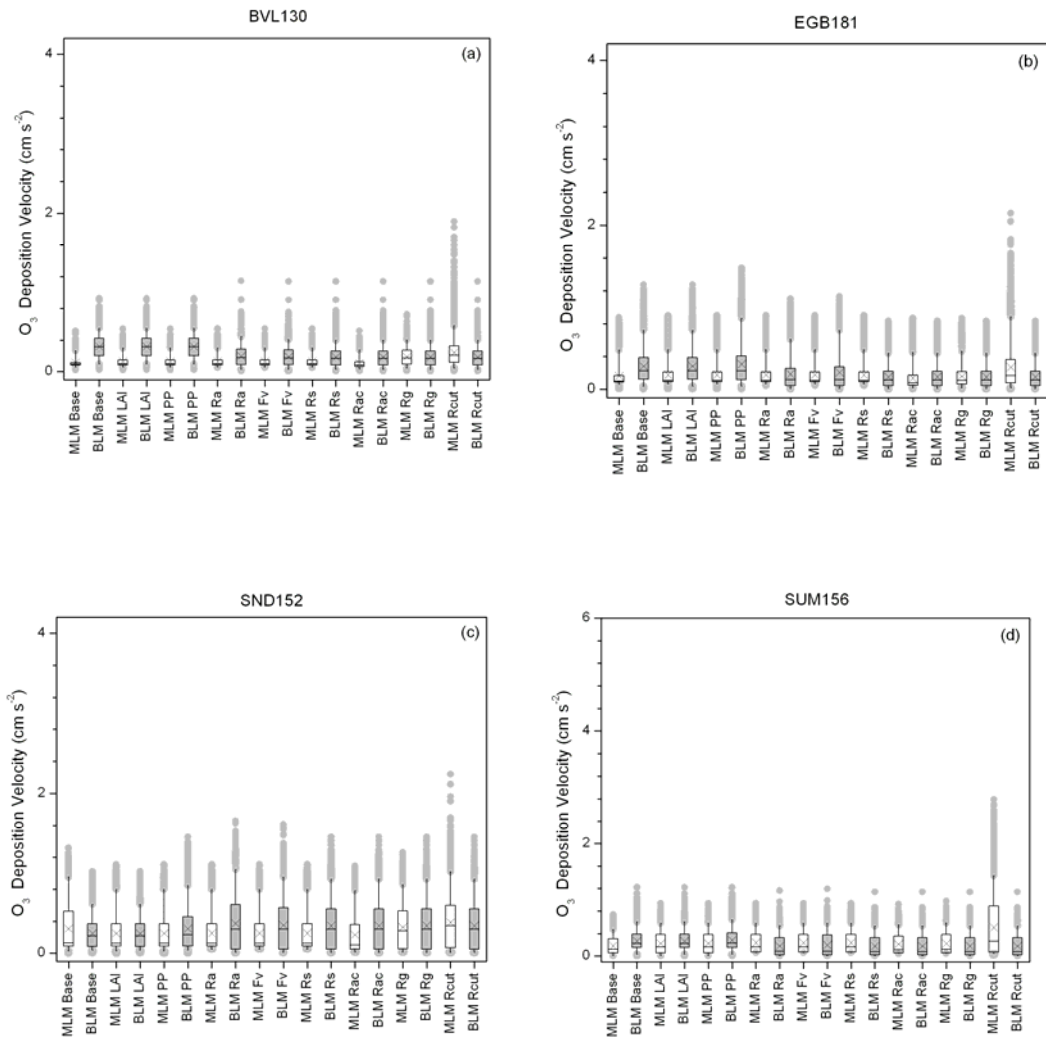


Figure 2. Ozone deposition velocity distributions for (a) BVL130, (b) EGB181, (c) SND152, and (d) SUM156 for different model configurations. White bars indicate values from MLM and grey bars indicate values from BLM. The abbreviations for the model configurations (x-axis) are provided in Table 1.

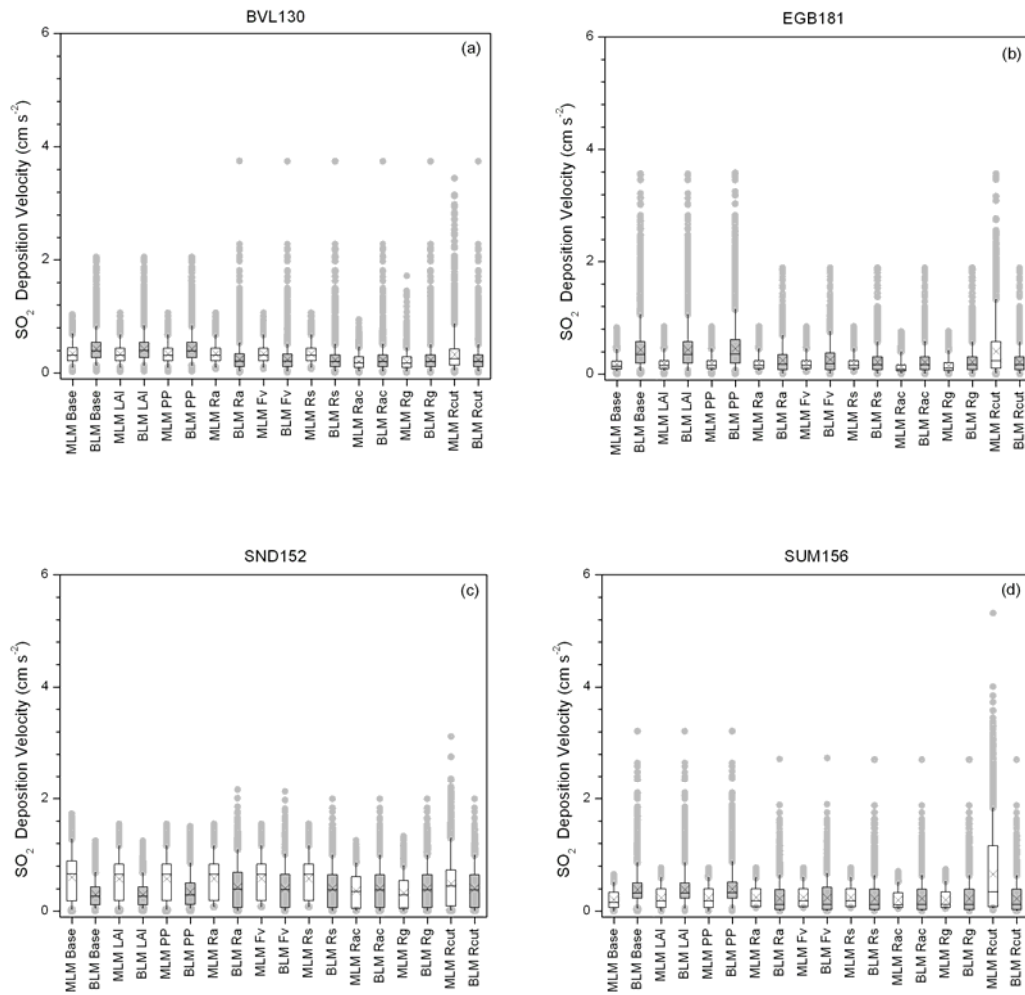


Figure 3. Sulfur dioxide deposition velocity distributions for (a) BVL130, (b) EGB181, (c) SND152, and (d) SUM156 for different model configurations. White bars indicate values from MLM and grey bars indicate values from BLM. The abbreviations for the model configurations (x-axis) are provided in Table 1.

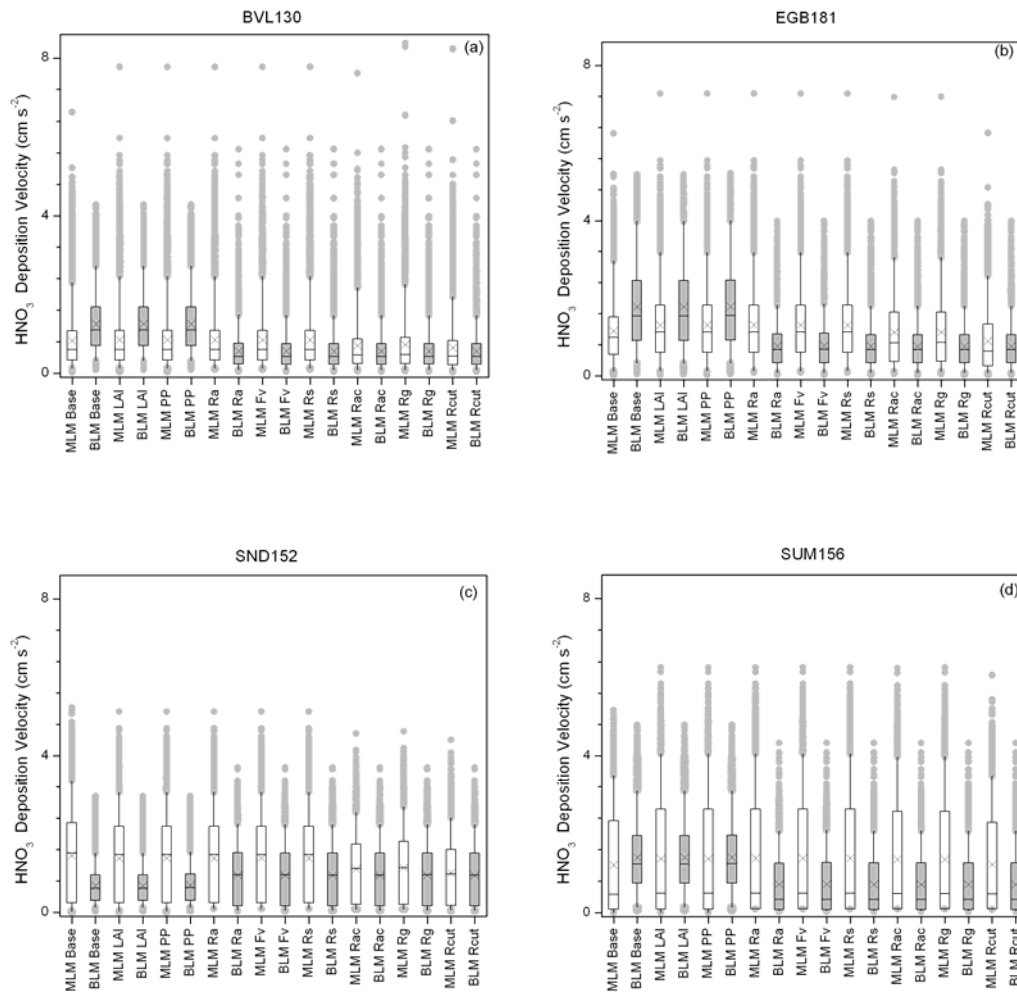


Figure 4. Nitric acid deposition velocity distributions for (a) BVL130, (b) EGB181, (c) SND152, and (d) SUM156 for different model configurations. White bars indicate values from MLM and grey bars indicate values from BLM. The abbreviations for the model configurations (x-axis) are provided in Table 1.

Table S1. Distribution of O<sub>3</sub> deposition velocities predicted by the MLM model for each run.

Site	Run Name	Mean	Minimum	Maximum	25 <sup>th</sup> Percentile	75 <sup>th</sup> Percentile
BVL130	Base	0.116	0.021	0.513	0.084	0.114
BVL130	LAI	0.129	0.021	0.541	0.085	0.147
BVL130	PP	0.129	0.021	0.541	0.085	0.147
BVL130	Ra	0.129	0.050	0.541	0.085	0.147
BVL130	Fv	0.129	0.050	0.541	0.085	0.147
BVL130	Rs	0.129	0.050	0.541	0.085	0.147
BVL130	Rac	0.109	0.012	0.515	0.065	0.126
BVL130	Rg	0.191	0.012	0.722	0.094	0.270
BVL130	Rcut	0.245	0.010	2.684	0.118	0.325
EGB181	Base	0.161	0.008	0.873	0.091	0.165
EGB181	LAI	0.177	0.008	0.900	0.094	0.209
EGB181	PP	0.177	0.008	0.900	0.094	0.209
EGB181	Ra	0.178	0.046	0.900	0.094	0.209
EGB181	Fv	0.178	0.046	0.900	0.094	0.209
EGB181	Rs	0.178	0.046	0.900	0.094	0.209
EGB181	Rac	0.137	0.003	0.866	0.052	0.171
EGB181	Rg	0.161	0.003	0.867	0.062	0.217
EGB181	Rcut	0.270	0.000	2.146	0.078	0.362
SND152	Base	0.307	0.000	1.313	0.092	0.526
SND152	LAI	0.248	0.000	1.110	0.088	0.368
SND152	PP	0.248	0.000	1.110	0.088	0.368
SND152	Ra	0.251	0.051	1.110	0.088	0.368
SND152	Fv	0.251	0.051	1.110	0.088	0.368
SND152	Rs	0.251	0.051	1.110	0.088	0.368
SND152	Rac	0.230	0.010	1.092	0.052	0.358
SND152	Rg	0.326	0.010	1.261	0.057	0.531
SND152	Rcut	0.384	0.002	2.239	0.068	0.598
SUM156	Base	0.185	0.005	0.739	0.056	0.306
SUM156	LAI	0.230	0.005	0.938	0.062	0.384
SUM156	PP	0.230	0.005	0.938	0.062	0.384
SUM156	Ra	0.239	0.063	0.938	0.074	0.384
SUM156	Fv	0.239	0.063	0.938	0.074	0.384
SUM156	Rs	0.239	0.063	0.938	0.074	0.384
SUM156	Rac	0.213	0.048	0.924	0.058	0.354
SUM156	Rg	0.224	0.048	0.982	0.058	0.382
SUM156	Rcut	0.508	0.010	4.062	0.071	0.891

Table S2. Distribution of O<sub>3</sub> deposition velocities predicted by the BLM model for each run.

Site	Run Name	Mean	Minimum	Maximum	25 <sup>th</sup> Percentile	75 <sup>th</sup> Percentile
BVL130	Base	0.317	0.026	0.922	0.203	0.420
BVL130	LAI	0.317	0.026	0.922	0.203	0.420
BVL130	PP	0.317	0.026	0.922	0.203	0.420
BVL130	Ra	0.198	0.006	1.146	0.089	0.285
BVL130	Fv	0.191	0.006	1.137	0.089	0.276
BVL130	Rs	0.184	0.006	1.137	0.087	0.263
BVL130	Rac	0.184	0.006	1.137	0.087	0.263
BVL130	Rg	0.184	0.006	1.137	0.087	0.263
BVL130	Rcut	0.184	0.006	1.137	0.087	0.263
EGB181	Base	0.281	0.004	1.273	0.121	0.389
EGB181	LAI	0.281	0.004	1.273	0.121	0.389
EGB181	PP	0.306	0.004	1.475	0.119	0.407
EGB181	Ra	0.186	0.001	1.100	0.047	0.254
EGB181	Fv	0.206	0.001	1.129	0.047	0.273
EGB181	Rs	0.153	0.001	0.833	0.046	0.220
EGB181	Rac	0.153	0.001	0.833	0.046	0.220
EGB181	Rg	0.153	0.001	0.833	0.046	0.220
EGB181	Rcut	0.153	0.001	0.833	0.046	0.220
SND152	Base	0.250	0.002	1.024	0.085	0.368
SND152	LAI	0.250	0.002	1.024	0.085	0.368
SND152	PP	0.307	0.002	1.454	0.088	0.455
SND152	Ra	0.373	0.002	1.656	0.050	0.606
SND152	Fv	0.351	0.002	1.612	0.050	0.567
SND152	Rs	0.344	0.002	1.453	0.050	0.554
SND152	Rac	0.344	0.002	1.453	0.050	0.554
SND152	Rg	0.344	0.002	1.453	0.050	0.554
SND152	Rcut	0.344	0.002	1.453	0.050	0.554
SUM156	Base	0.271	0.003	1.218	0.155	0.388
SUM156	LAI	0.271	0.003	1.218	0.155	0.388
SUM156	PP	0.284	0.003	1.218	0.158	0.410
SUM156	Ra	0.180	0.002	1.163	0.021	0.331
SUM156	Fv	0.198	0.002	1.196	0.021	0.377
SUM156	Rs	0.180	0.002	1.140	0.021	0.330
SUM156	Rac	0.180	0.002	1.140	0.021	0.330
SUM156	Rg	0.180	0.002	1.140	0.021	0.330
SUM156	Rcut	0.180	0.002	1.140	0.021	0.330

Table S3. Distribution of SO<sub>2</sub> deposition velocities predicted by the MLM model for each run.

Site	Run Name	Mean	Minimum	Maximum	25 <sup>th</sup> Percentile	75 <sup>th</sup> Percentile
BVL130	Base	0.347	0.023	1.031	0.220	0.448
BVL130	LAI	0.342	0.023	1.063	0.218	0.440
BVL130	PP	0.342	0.023	1.063	0.218	0.440
BVL130	Ra	0.343	0.072	1.063	0.218	0.440
BVL130	Fv	0.343	0.072	1.063	0.218	0.440
BVL130	Rs	0.343	0.072	1.063	0.218	0.440
BVL130	Rac	0.208	0.011	0.944	0.101	0.290
BVL130	Rg	0.205	0.011	1.716	0.099	0.287
BVL130	Rcut	0.329	0.011	5.794	0.140	0.425
EGB181	Base	0.181	0.008	0.823	0.092	0.231
EGB181	LAI	0.193	0.008	0.845	0.100	0.241
EGB181	PP	0.193	0.008	0.845	0.100	0.241
EGB181	Ra	0.194	0.046	0.845	0.100	0.241
EGB181	Fv	0.194	0.046	0.845	0.100	0.241
EGB181	Rs	0.194	0.046	0.845	0.100	0.241
EGB181	Rac	0.132	0.002	0.758	0.056	0.164
EGB181	Rg	0.152	0.002	0.761	0.063	0.204
EGB181	Rcut	0.409	0.001	3.573	0.110	0.575
SND152	Base	0.603	0.000	1.732	0.185	0.887
SND152	LAI	0.573	0.000	1.552	0.189	0.838
SND152	PP	0.573	0.000	1.552	0.189	0.838
SND152	Ra	0.579	0.074	1.552	0.189	0.838
SND152	Fv	0.579	0.074	1.552	0.189	0.838
SND152	Rs	0.579	0.074	1.552	0.189	0.838
SND152	Rac	0.362	0.010	1.257	0.052	0.612
SND152	Rg	0.325	0.010	1.331	0.052	0.542
SND152	Rcut	0.489	0.003	3.116	0.091	0.731
SUM156	Base	0.207	0.005	0.653	0.064	0.339
SUM156	LAI	0.240	0.005	0.772	0.068	0.398
SUM156	PP	0.240	0.005	0.772	0.068	0.398
SUM156	Ra	0.250	0.062	0.772	0.077	0.398
SUM156	Fv	0.250	0.062	0.772	0.077	0.398
SUM156	Rs	0.250	0.062	0.772	0.077	0.398
SUM156	Rac	0.198	0.048	0.705	0.064	0.327
SUM156	Rg	0.204	0.048	0.743	0.064	0.346
SUM156	Rcut	0.656	0.018	5.314	0.081	1.158

Table S4. Distribution of SO<sub>2</sub> deposition velocities predicted by the BLM model for each run.

Site	Run Name	Mean	Minimum	Maximum	25 <sup>th</sup> Percentile	75 <sup>th</sup> Percentile
BVL130	Base	0.426	0.032	2.045	0.271	0.541
BVL130	LAI	0.427	0.032	2.045	0.271	0.542
BVL130	PP	0.426	0.032	2.045	0.271	0.542
BVL130	Ra	0.246	0.011	3.749	0.115	0.345
BVL130	Fv	0.240	0.011	3.744	0.115	0.333
BVL130	Rs	0.235	0.011	3.744	0.113	0.323
BVL130	Rac	0.235	0.011	3.744	0.113	0.323
BVL130	Rg	0.235	0.011	3.744	0.113	0.323
BVL130	Rcut	0.235	0.011	3.744	0.113	0.323
EGB181	Base	0.436	0.006	3.571	0.196	0.576
EGB181	LAI	0.436	0.006	3.571	0.196	0.576
EGB181	PP	0.456	0.006	3.585	0.195	0.615
EGB181	Ra	0.245	0.002	1.888	0.082	0.348
EGB181	Fv	0.262	0.002	1.888	0.082	0.378
EGB181	Rs	0.218	0.002	1.885	0.081	0.308
EGB181	Rac	0.218	0.002	1.885	0.081	0.307
EGB181	Rg	0.218	0.002	1.885	0.081	0.308
EGB181	Rcut	0.218	0.002	1.885	0.081	0.308
SND152	Base	0.297	0.005	1.249	0.117	0.432
SND152	LAI	0.297	0.005	1.249	0.117	0.432
SND152	PP	0.344	0.005	1.507	0.120	0.503
SND152	Ra	0.428	0.003	2.157	0.068	0.687
SND152	Fv	0.410	0.003	2.127	0.068	0.656
SND152	Rs	0.405	0.003	1.994	0.067	0.651
SND152	Rac	0.405	0.003	1.994	0.067	0.651
SND152	Rg	0.405	0.003	1.994	0.067	0.651
SND152	Rcut	0.404	0.003	1.994	0.067	0.651
SUM156	Base	0.385	0.005	3.212	0.235	0.500
SUM156	LAI	0.385	0.005	3.212	0.235	0.500
SUM156	PP	0.395	0.005	3.212	0.235	0.516
SUM156	Ra	0.224	0.003	2.715	0.033	0.387
SUM156	Fv	0.238	0.003	2.732	0.033	0.427
SUM156	Rs	0.224	0.003	2.704	0.033	0.389
SUM156	Rac	0.224	0.003	2.704	0.033	0.389
SUM156	Rg	0.224	0.003	2.704	0.033	0.389
SUM156	Rcut	0.224	0.003	2.704	0.033	0.389

Table S5. Distribution of HNO<sub>3</sub> deposition velocities predicted by the MLM model for each run.

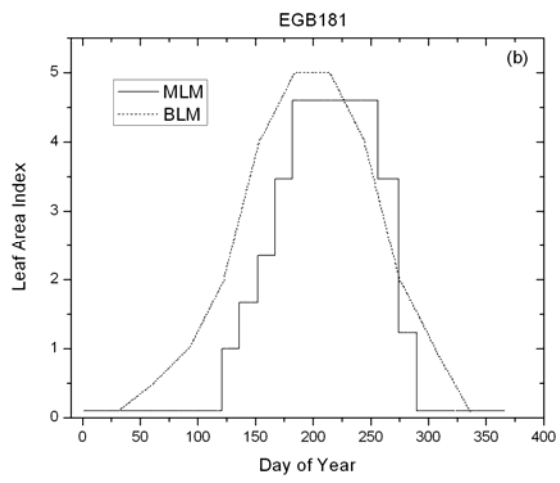
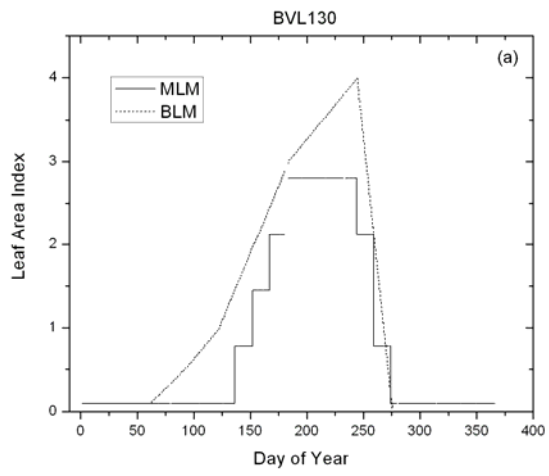
Site	Run Name	25 <sup>th</sup>	75 <sup>th</sup>
------	----------	------------------	------------------

		Mean	Minimum	Maximum	Percentile	Percentile
BVL130	Base	0.827	0.024	6.629	0.335	1.074
BVL130	LAI	0.848	0.024	7.775	0.334	1.087
BVL130	PP	0.848	0.024	7.775	0.334	1.087
BVL130	Ra	0.849	0.094	7.775	0.334	1.087
BVL130	Fv	0.849	0.094	7.775	0.334	1.087
BVL130	Rs	0.849	0.094	7.775	0.334	1.087
BVL130	Rac	0.700	0.050	7.615	0.245	0.864
BVL130	Rg	0.725	0.050	8.384	0.247	0.907
BVL130	Rcut	0.643	0.018	8.242	0.215	0.833
EGB181	Base	1.148	0.008	6.251	0.547	1.506
EGB181	LAI	1.302	0.008	7.272	0.601	1.816
EGB181	PP	1.302	0.008	7.272	0.601	1.816
EGB181	Ra	1.303	0.082	7.272	0.601	1.816
EGB181	Fv	1.303	0.082	7.272	0.601	1.816
EGB181	Rs	1.303	0.082	7.272	0.601	1.816
EGB181	Rac	1.118	0.036	7.184	0.368	1.639
EGB181	Rg	1.120	0.036	7.196	0.369	1.640
EGB181	Rcut	0.891	0.007	6.259	0.256	1.328
SND152	Base	1.446	0.000	5.234	0.245	2.286
SND152	LAI	1.375	0.000	5.131	0.244	2.188
SND152	PP	1.375	0.000	5.131	0.244	2.188
SND152	Ra	1.382	0.091	5.131	0.244	2.188
SND152	Fv	1.382	0.091	5.131	0.244	2.188
SND152	Rs	1.382	0.091	5.131	0.244	2.188
SND152	Rac	1.103	0.072	4.571	0.207	1.739
SND152	Rg	1.141	0.072	4.625	0.207	1.803
SND152	Rcut	1.004	0.018	4.407	0.175	1.599
SUM156	Base	1.212	0.005	5.173	0.086	2.331
SUM156	LAI	1.369	0.005	6.263	0.087	2.632
SUM156	PP	1.369	0.005	6.263	0.087	2.632
SUM156	Ra	1.383	0.093	6.263	0.095	2.632
SUM156	Fv	1.383	0.093	6.263	0.095	2.632
SUM156	Rs	1.383	0.093	6.263	0.095	2.632
SUM156	Rac	1.355	0.091	6.243	0.094	2.569
SUM156	Rg	1.355	0.091	6.258	0.094	2.569
SUM156	Rcut	1.221	0.071	6.060	0.093	2.292

Table S6. Distribution of HNO<sub>3</sub> deposition velocities predicted by the BLM model for each run.

Site	Run Name	Mean	Minimum	Maximum	25 <sup>th</sup> Percentile	75 <sup>th</sup> Percentile
------	----------	------	---------	---------	-----------------------------	-----------------------------

BVL130	Base	1.253	0.090	4.288	0.701	1.677
BVL130	LAI	1.253	0.090	4.288	0.701	1.677
BVL130	PP	1.253	0.090	4.288	0.701	1.677
BVL130	Ra	0.563	0.035	5.697	0.230	0.757
BVL130	Fv	0.561	0.035	5.697	0.229	0.753
BVL130	Rs	0.560	0.035	5.697	0.229	0.752
BVL130	Rac	0.560	0.035	5.697	0.229	0.752
BVL130	Rg	0.560	0.035	5.697	0.230	0.753
BVL130	Rcut	0.560	0.035	5.697	0.229	0.753
EGB181	Base	1.772	0.036	5.200	0.912	2.446
EGB181	LAI	1.772	0.036	5.200	0.912	2.446
EGB181	PP	1.781	0.036	5.221	0.915	2.461
EGB181	Ra	0.768	0.011	3.995	0.332	1.076
EGB181	Fv	0.777	0.011	3.995	0.332	1.095
EGB181	Rs	0.758	0.011	3.995	0.329	1.059
EGB181	Rac	0.758	0.011	3.995	0.329	1.058
EGB181	Rg	0.758	0.011	3.995	0.329	1.059
EGB181	Rcut	0.758	0.011	3.995	0.329	1.059
SND152	Base	0.679	0.023	2.958	0.304	0.956
SND152	LAI	0.679	0.023	2.958	0.304	0.956
SND152	PP	0.693	0.023	2.958	0.307	0.979
SND152	Ra	0.950	0.018	3.707	0.162	1.519
SND152	Fv	0.944	0.018	3.707	0.162	1.509
SND152	Rs	0.943	0.018	3.707	0.161	1.508
SND152	Rac	0.943	0.018	3.707	0.161	1.509
SND152	Rg	0.943	0.018	3.707	0.161	1.509
SND152	Rcut	0.943	0.018	3.707	0.162	1.508
SUM156	Base	1.405	0.039	4.796	0.750	1.955
SUM156	LAI	1.405	0.039	4.796	0.750	1.955
SUM156	PP	1.409	0.039	4.796	0.750	1.964
SUM156	Ra	0.713	0.022	4.332	0.075	1.259
SUM156	Fv	0.720	0.022	4.332	0.075	1.274
SUM156	Rs	0.715	0.022	4.332	0.075	1.263
SUM156	Rac	0.715	0.022	4.332	0.075	1.263
SUM156	Rg	0.715	0.022	4.332	0.075	1.263
SUM156	Rcut	0.715	0.022	4.332	0.075	1.263



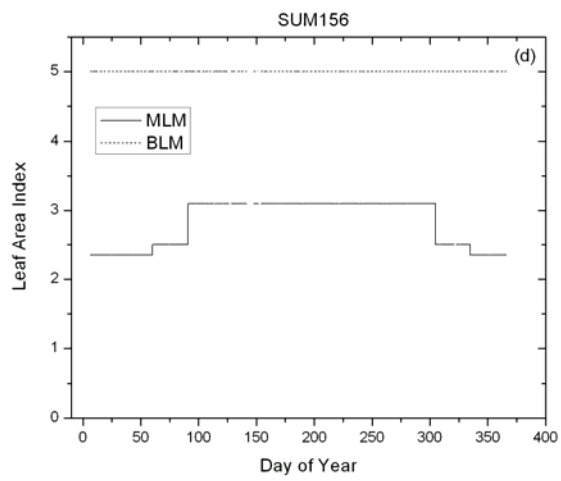
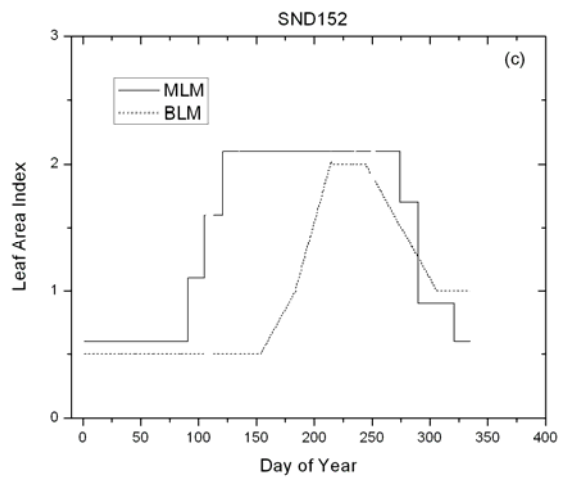
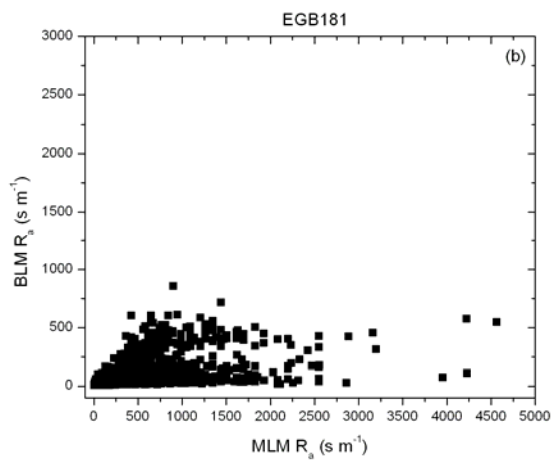
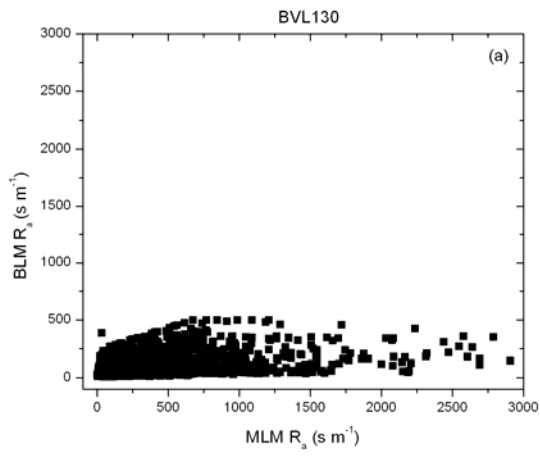


Figure S1. Time series of leaf area index for (a) BVL130, (b) EGB181, (c) SND152, and (d) SUM156.



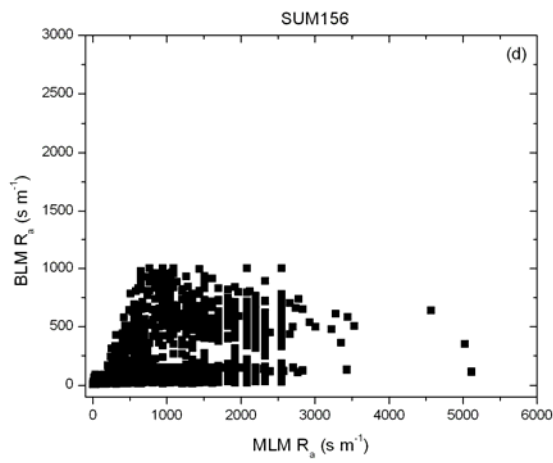
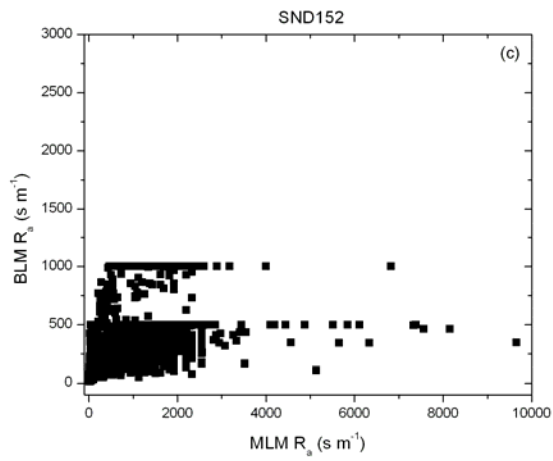
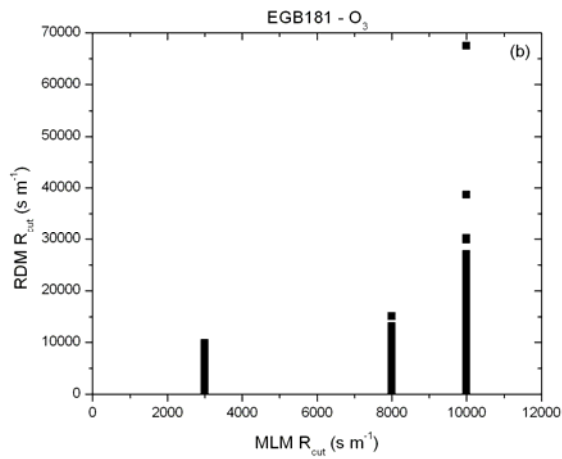
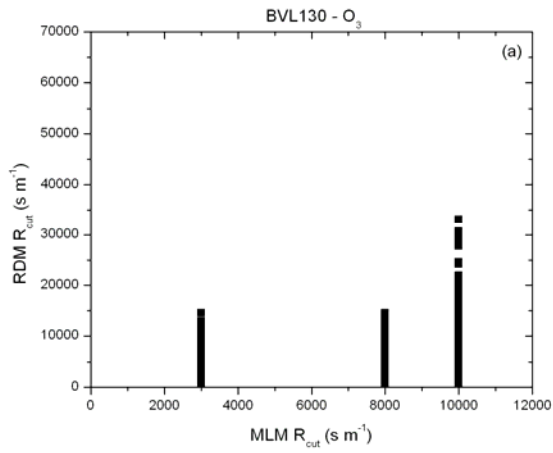


Figure S2. Scatter plot of aerodynamic resistance ( $s m^{-1}$ ) calculated by MLM and BLM for (a) BVL130, (b) EGB181, (c) SND152, and (d) SUM156.



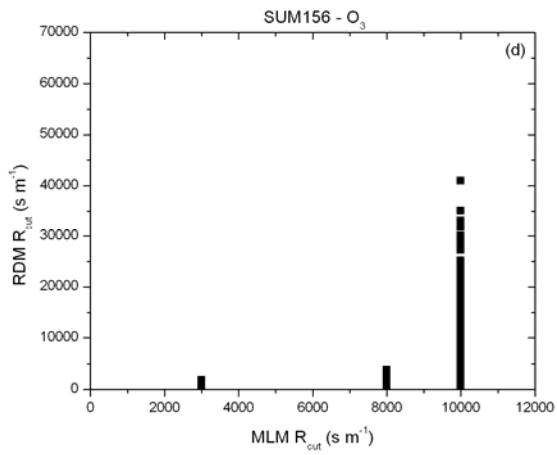
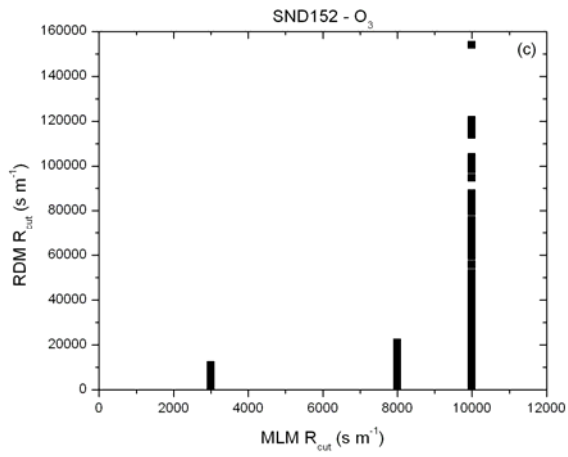
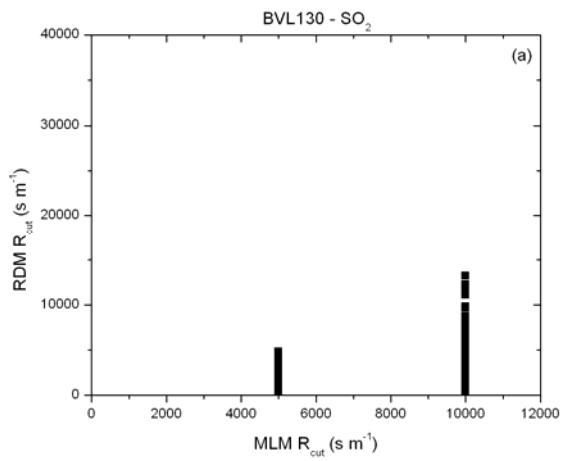
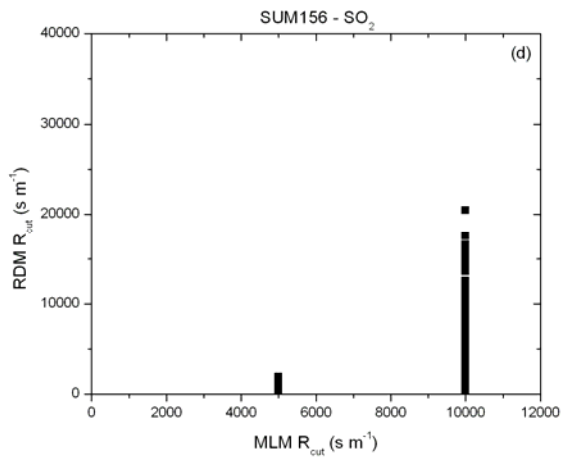


Figure S3. Scatter plot of cuticular resistance (s m<sup>-1</sup>) for O<sub>3</sub> calculated by MLM and BLM for (a) BVL130, (b) EGB181, (c) SND152, and (d) SUM156.



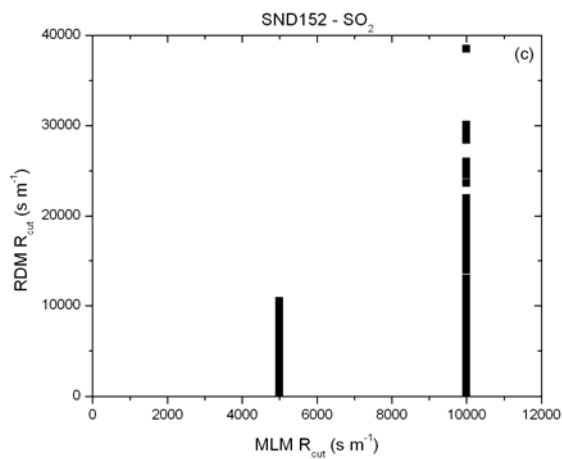
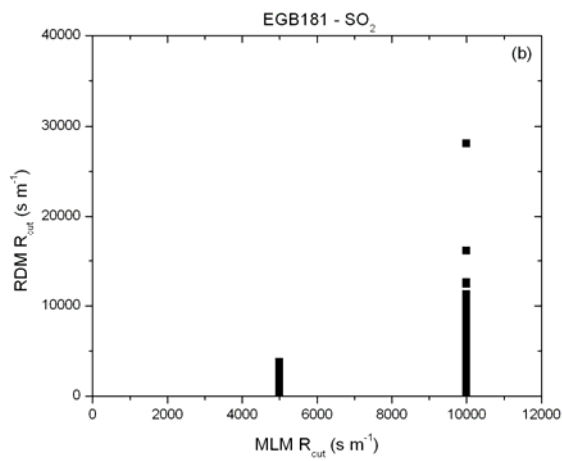


Figure S4. Scatter plot of cuticular resistance ( $\text{s m}^{-1}$ ) for  $\text{SO}_2$  calculated by MLM and BLM for (a) BVL130, (b) EGB181, (c) SND152, and (d) SUM156.